

# Design of Full-Duplex Millimeter-Wave Integrated Access and Backhaul Networks

Junkai Zhang, *Student Member, IEEE*, Navneet Garg, *Member, IEEE*, Mark Holm, *Member, IEEE*,  
and Tharmalingam Ratnarajah, *Senior Member, IEEE*

## ABSTRACT

One of the key technologies for the future cellular networks is full-duplex (FD) enabled Integrated Access and Backhaul (IAB) networks operating in the millimeter-wave (mmWave) frequencies. The main challenge in realizing the FD-IAB networks is mitigating the impact of self-interference (SI) in the wideband mmWave frequencies. In this article, we first introduce the 3GPP IAB network architectures and wideband mmWave channel models. By utilizing the subarray-based hybrid precoding scheme, at the FD-IAB-node, multiuser interference is mitigated using zero-forcing (ZF) at the transmitter, whereas the residual SI after successfully deploying antenna and analog cancellation is canceled by minimum mean square error (MMSE) baseband combiner at the receiver. The spectral efficiency (SE) is evaluated for the RF insertion loss (RFIL) with different kinds of phase shifters and the channel uncertainty. Simulation results show that, in the presence of the RFIL, the almost double SE, which is close to that obtained from fully connected hybrid precoding, can be achieved as compared with half-duplex systems, when the uncertainties are of low strength.

## INTRODUCTION

The key technologies, namely, millimeter-wave (mmWave) wideband communications, full-duplex (FD) transmissions, and Integrated Access and Backhaul (IAB) networks, are emerging as the backbone of 5G and beyond communications. A large bandwidth provided by mmWave systems can be exploited for wideband transmissions to increase data rates, which are orders of magnitude more than that of the current microwave systems. However, a beamformed array with a large number of antennas is needed to compensate for the higher path loss at mmWave frequencies [1]. Moreover, to enhance the coverage, dense deployment of multi-antenna access points has been considered as a promising approach. However, providing traditional fiber backhauling connection to all these small cells is not possible both economically and

physically. To address this issue, 3GPP proposed cost-effective dense deployment of wireless backhauling through IAB-nodes to achieve promising gains even under higher mobile data traffic [2].

Moreover, to leverage the full benefits of IAB networks with the mmWave wideband, the IAB-nodes are set to operate in the FD mode. Compared with the half-duplex (HD) transmission, FD can enhance the spectral efficiency (SE) and reduce the communication delay without any requirement for the guard time/band [3]. Unlike traditional microwave communications, where full digital baseband (BB) precoding schemes are sufficient, the hybrid precoding is essential in mmWave communications [1]. For wideband mmWave-FD-IAB networks, the hardware efficient subarray based hybrid precoding is adopted in this article.

Since in a FD-IAB network, the access and the backhaul communications occur at the same time-frequency resource, it naturally gives rise to self-interference (SI) at the receiver of the FD-IAB-node. Typically, the magnitude of the SI can be more than 100 dB, which is much stronger than the signal of interest, as studied in [4]. Such a high SI power can significantly exceed the hardware dynamic range and distort the benefits of FD transmission. Thus, it is important to reduce SI power before the down-conversion. In the microwave communications, successful SI cancellation (SIC) can be achieved at the antenna domain (i.e., by deploying special antenna isolation), the RF domain (i.e., by replicating the SI channel and subtracting it from the received signal), and the digital domain (i.e., by canceling the residual SI (RSI) after RF cancellation by beamformer design). Usually, a combination of these stages has shown satisfactory results [3], which we also expect to provide a good solution for the mmWave wideband communications. In this article, we mainly focus on the design of the digital cancellation, where the antenna isolation and the RF cancellation are assumed to be successfully achieved. Therefore, only the RSI signal will be handled in the digital domain.

In this article, we first introduce the fundamental 3GPP network architectures for the FD-IAB systems, followed by the description of the general mmWave and the SI channel models. Next, a hybrid analog/digital transceiver design via the cost-efficient subarray structure for the multiuser scenario is explained. The multiuser interference (MUI) at the transmitter of the IAB-node and the RSI at the receiver of the IAB-node are mitigated by zero-forcing (ZF) and minimum mean squared error (MMSE) in the digital BB domain, respectively. Further, the performance limitations of FD enabled multiuser

This work was accepted for publication in the special issue of Full Duplex Communications Theory, Standardization and Practice, in IEEE Wireless Communications, February, 2021. Manuscript received May 13, 2020; revised September 3, 2020; accepted October 19, 2020. Date of current version December 15, 2020.

J. Zhang, N. Garg, and T. Ratnarajah are with Institute for Digital Communications, The University of Edinburgh, Edinburgh, EH9 3FG, UK (e-mail: {jzhang15, ngarg, T. Ratnarajah}@ed.ac.uk).

M. Holm is with Radio Basestation Systems Department, Huawei Technologies (Sweden) AB, Gothenburg, Sweden. (e-mail: mark.holm@huawei.com).

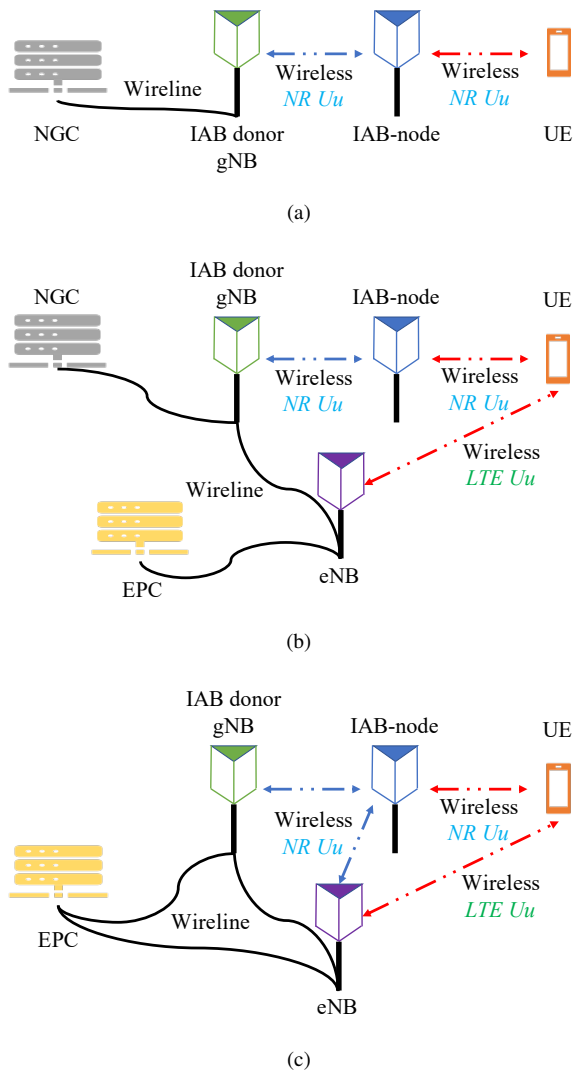


Fig. 1. Examples for IAB-FD network architectures operating in SA mode and NSA mode: a) UE: SA with NGC, IAB-node: SA with NGC; b) UE: NSA with EPC, IAB-node: SA with NGC; c) UE: NSA with EPC, IAB-node: NSA with EPC.

mmWave-IAB networks under subarray hybrid precoding structure are studied in the presence of the RF insertion loss (RFIL) and the channel estimation error (CEE). With the RFIL, simulations show that the SE performance of the fully connected hybrid precoding structure is similar to that for the subarray-based hybrid precoding structure. Moreover, as the CEE increases, the rate improvement of FD over HD decreases. Besides, the SE intersection point of FD and HD that appears at the backhaul link enables the understanding of the maximum achievable digital cancellation, which will encourage the development of advanced hybrid transceivers with efficient resource allocation schemes in the future.

### 3GPP NETWORK ARCHITECTURES

The 3rd Generation Partnership Project (3GPP) release 16 explores the standards for 5G new radio (NR) communications. IAB architectures, radio protocols, and physical layer aspects related to relaying of access traffic by sharing radio resources between access and backhaul links are investigated

in the technical specification TR 38.874 [5]. These initial studies show the benefits of in-band backhauling over out-of-band backhauling for access links. However, these fundamental results for FD operations are still in its infancy. Further, the knowledge of the impact of FD operations at mmWave frequencies is also limited, since the wideband channel model for FD operations still needs thorough investigation. According to the 3GPP specification in [5], the IAB systems are typically deployed in two modes, namely standalone (SA) mode, and non-standalone (NSA) mode, as shown in Fig. 1. In the SA mode shown in Fig. 1(a), the IAB-node connects to the 5G next-generation core (NGC) network via the IAB donor (gNB), and the UE also operates in the SA mode (i.e., it only connects to the IAB-node). In Fig. 1(b), the UE is connected in the NSA manner, while the IAB-node is in the SA mode. In this scenario, both the Long Term Evolution (LTE) radio and the NR can be used for the UE, and NR links are utilized for backhauling. Further, if the IAB-node works in the NSA mode, it is also connected to the eNB nodes (i.e., the 4G base stations), as shown in Fig. 1(c). Thus, a UE in the NSA mode can choose to connect the IAB-connected-eNB or different one. In the third scenario, the IAB-node can utilize the LTE links for initial access, route selection, etc.

A multihop mmWave IAB networks in SA mode is shown in Fig. 2(a). In this figure, there are three kinds of nodes listed as follows,

- A single logical IAB donor, which is the source node, also known as the gNB. It takes the responsibility of functionality and splits according to the 3GPP NG-RAN architecture [6]. Usually, the gNB has a wired connection to the core network (NGC) and has wireless connections to other nodes.
- IAB-nodes, which wirelessly communicate with both backhaul and access links, provide FD operations, and perform IAB specific tasks such as resource allocation, route selection, and optimization. The IAB-nodes can be connected to other HD-IAB-nodes or FD-IAB-nodes.
- UE nodes, which request and receive the contents via FD or HD operation. Since UEs operate in the SA mode, they only connect to the IAB-nodes.

Typically, the IAB-node enables not only UEs but also other FD/HD-IAB-nodes to communicate with the gNB. In the SA architecture illustrated in Fig 2(a), IAB-nodes forward the backhaul traffic to the core network in different spectrum, whereas with this general star topology, Taghizadeh *et al.* [7] consider a central station delivering the backhaul traffic from multiple nodes, which may require efficient interference management schemes.

There are two kinds of topology models to characterize such multihop networks. The first one is the spanning tree (ST) model, where one IAB-node connects to only one parent node (i.e., the IAB donor or another IAB-node). The second model uses the directed acyclic graphs (DAG), where one IAB-node has multiple parent nodes, or has multiple routes to one parent node, or a combination of these two cases. [5], [8]. These ST and DAG models for Fig. 2(a) are difficult to analyze from the physical layer perspective. Thus, for the

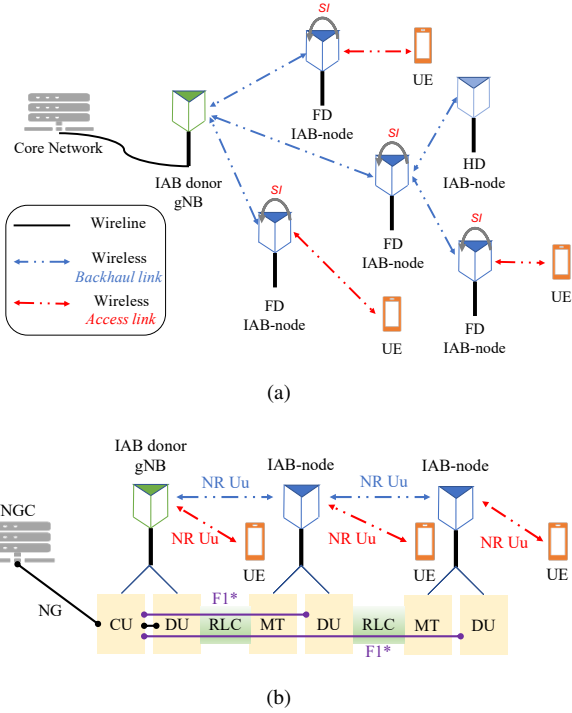


Fig. 2. a) Illustration of multihop mmWave-FD-IAB network architecture diagram in SA mode; b) CU/DU split architecture for multihop IAB system.

multihop IAB networks, a simplified version, i.e., the Central Unit (CU)/Distributed Unit (DU) split architecture is preferred in studies [2], [8], and is shown in Fig. 2(b), where the CU and the DU represent external interfaces of the node. In this architecture, the IAB-node has two NR functional units, viz., the Mobile Termination (MT) unit, which controls the upstream link connection with the IAB donor or the IAB-node; and the DU, which provides connections to UEs or MTs on other IAB-nodes of the downstream link. The IAB donor has two functional units as well, viz., the CU is responsible for serving the DUs on all IAB-nodes and the donor itself, while the DU provides support to the UEs and the MTs on all IAB-nodes. The F1\* function connects the interface of the IAB-node to the interface of the IAB donor. It runs on the Radio Link Control (RLC) channels, representing the connections between the DU and the downlink MT or UEs.

## CHANNEL MODELS

### General mmWave Channel

The mmWave channel has several characteristics that differentiate it from the traditional microwave channels, such as higher path loss (owing to higher operating frequencies), the spatial selectivity (due to high path losses and beamforming), and increased correlation among antennas (due to densely collocated arrays). These distinctive characteristics imply that the statistical fading distributions such as the Rayleigh distribution, used in traditional wireless channels become inaccurate, since the number of fading paths is small. Hence, the mmWave channel between two different nodes is likely modeled as a geometric wideband frequency selective

channel according to the extended Saleh-Valenzuela model, studied in [1], [9].

An Orthogonal Frequency Division Multiplexing (OFDM) system with  $K$  subcarriers is adopted, where  $D$  cyclic prefix (CP) is added to avoid the Inter Symbol Interference (ISI). For each of the  $D$  taps of the wideband channel, scatterers in the area contribute to multiple propagation paths. These reflected multipath components (rays) arrive in clusters, which cause the sparse nature in the channel response. The value of the  $d$ th tap of the channel is modeled using the product of the complex random gain, the complex exponential of angles of arrival and departure (AoAs/AoDs), and the pulse-shaping filter. The complex random gain of each ray has the magnitude following the Rayleigh distribution with the parameter defined by the number of total paths. For the uniform planar arrays (UPAs), the central azimuth AoAs/AoDs of fading paths (rays) in each cluster are uniformly distributed in  $[-\pi, \pi]$ , and the corresponding central elevation AoAs/AoDs are uniformly distributed in  $[-\pi/2, \pi/2]$ . In each cluster, these azimuth and elevation angles of the rays are assumed to have the Laplacian distribution with a given angle spread. The raised cosine pulse shaping filter is utilized with sampling time  $T_s$ , evaluated at  $dT_s - \tau_{c,l}$  seconds, where  $\tau_{c,l}$  is the path delay of the  $l$ th ray in the  $c$ th cluster and is uniformly distributed in  $[0, DT_s]$ . The close-in (CI) path loss model with a reference distance of 1m is introduced to capture the average path loss. Ultimately, the channel at subcarrier  $k = 1, 2, \dots, K$  is given by the discrete Fourier transform (DFT) of the delay- $d$  channel.

### Self-Interference Channel

The FD-IAB-node is comprised of a transmit antenna array and a receive antenna array. In FD operations, a mmWave SI channel is defined as the mmWave channel between the transmit antenna and the receiver antenna at the IAB-node. Through measurements, the mmWave SI channel is verified to have both line-of-sight (LOS) and non-line-of-sight (NLOS) components [4]. The LOS component accounts for a deterministic direct path loss. Its strength is very high due to a very short distance between the transceiver of the IAB-node and is assumed to adopt a near-field model, since the distance between the transceiver is smaller than  $2D^2/\lambda$ , where  $D$  is the antenna aperture diameter, and  $\lambda$  is the wavelength [3]. The coefficient of the LOS channel matrix depends on the distance between the individual elements of the transceiver. The NLOS component indicates random components caused by reflections from obstacles around the IAB-node, where the general mmWave channel model may be acceptable, except with a smaller number of rays. A Rician-like channel model could be utilized to model the SI channel due to a strong LOS path. A detailed hypothetical wideband mmWave SI channel model is formulated in our recent work [10]. It is worth noting that there is still ambiguity in characterizing the mmWave SI channel model in the literature.

A study in [3] shows that the resulting SI channel is sparse and low rank. Unfortunately, as mentioned in [11], the difficulties of SIC arises due to its inability to cancel the NLOS component of the SI signal by the three-stage

SIC scheme. It is due to the fact that the present SI channel estimation methods have proved to be inaccurate due to the strong antenna correlation in the near-field region. Moreover, in general, the channel estimation for microwave communications assumes the steady oscillator phase noise (PN), however, for mmWave communications, this assumption can cause large estimation error, since the PN changes rapidly and cannot be ignored. In [11], with the Rician SI channel model, a joint SI channel and PN estimation algorithm for mmWave communications using the Kalman filter is proposed, which is shown to achieve its mean squared error (MSE) lower bound successfully. With their efficient estimator, the RSI can be decreased to an acceptable amount.

The CEE,  $\Delta_{\text{SI}}[k]$ , is introduced to model the imperfect RF effective SI channel and analyze the corresponding system performance. The perfect RF effective SI channel (i.e., the product of the RF combiner, the SI channel matrix, and the RF precoder) at the  $k$ th subcarrier is assumed to be the sum of the estimated RF effective SI channel and the CEE. The CEE is assumed to be Gaussian with zero mean and small variance [12]. Note that the estimated effective channel after analog cancellation is used to design the precoders at transmitters and the combiners at receivers to cancel the remaining SI. However, interference leakage occurs due to the CEE and results in the RSI power. The impact of the CEE on the system capacity is given in the later section.

#### HYBRID TRANSCEIVER DESIGN

Since the wideband channel is frequency selective, each node adopts an OFDM system, ensuring that each subcarrier experiences a flat-fading channel. In conventional MIMO networks, only BB beamforming has been used to maximize the SE, provided that each node has a fully connected RF chain corresponding to each antenna. However, in mmWave communications, the small aperture size of the antenna and the large array size make it impossible for each antenna to have an RF chain. Thus, hybrid precoding has been utilized with a much lesser number of RF chains than the number of antennas, e.g., for gNB with 256 antennas, the number of RF chains is set to 4. For the wideband channel, we assume the BB beamforming is different for each subcarrier and is based on the number of RF chains and that of data streams. In contrast, the RF beamforming is achieved via phase shifters (PSs) and is the same for all subcarriers. The dimension of the RF beamforming is defined by the number of RF chains and the length of the antenna array. There are two kinds of hybrid transceiver structures studied in [1],

- Fully connected, where each RF chain connects to each antenna, i.e., all the antennas are connected to each of the RF chains.
- Partially connected (or subarray), where each RF chain only connects to a disjoint subset of antennas.

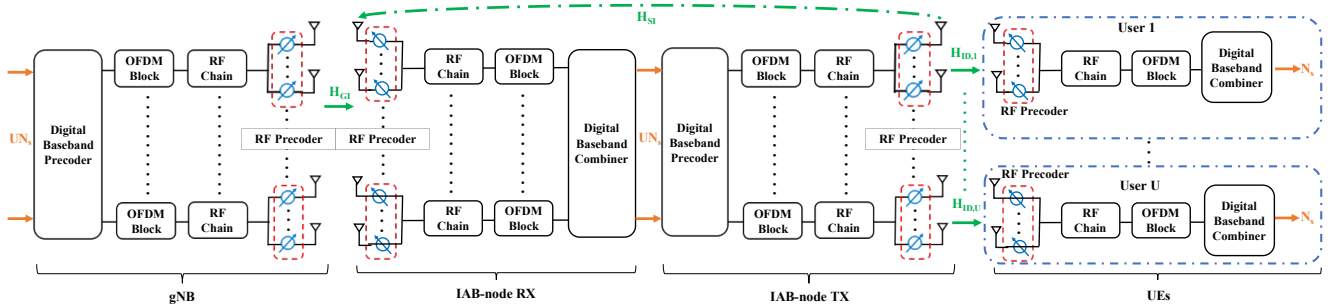
Although both structures employ fewer RF chains, the second structure is easier to deploy and more cost-efficient in practice. Since in a fully connected structure, mmWave antenna spacing and aperture size are small, which causes a high correlation between the outputs of RF chains. For the multiuser scenario,

each subarray is set to serve a single user, which means that the number of subarrays can be selected based on the number of users, see Fig. 3. In Fig. 3(b), each user is shown to be served by 1 subarray with 16 antenna arrays panel.

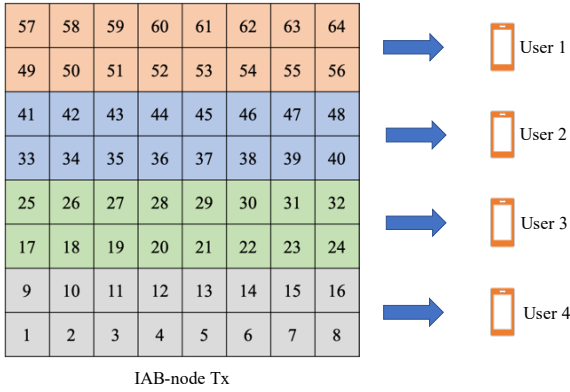
Fig. 3(a) gives the architecture of a multiuser hybrid transceiver for an IAB-FD wideband mmWave system, which is used for the analysis for the IAB networks in this work. For the transmitter side, the OFDM block performs the inverse DFT (IDFT) and adds the CP to the precoded streams using the BB precoder. On the receiver side, the OFDM block removes the CP and performs the DFT, followed by the BB combiner operation. Since each of the users (says  $U$  in total) communicates single data streams, the total number of data streams ( $N_s = U$ ) should not exceed the number of RF chains at the transmitter of the IAB-node.

Our objective in hybrid transceiver design is to maximize the SE across all subcarriers for access and backhaul links. This joint maximization problem concerning the RF and the BB precoders and combiners has a few constraints as follows. Since RF precoders and combiners are implemented using PSs, it poses the constraint that the magnitude of each entry of the RF precoder and combiner matrices should be precisely equal to 1. Further, the effective coupled RF and BB precoders must satisfy the transmit power constraint. Assuming equal power allocation across data streams, the squared norm of the hybrid precoder at each subcarrier should not exceed the length of the data stream vector. Since the maximization problem is non-convex due to coupled RF and BB variables, a joint optimal solution for these variables is intractable.

Interestingly, the near-optimal solution, where the RF and the BB variables are obtained separately, is studied in [1]. Ideally, the RF part of the hybrid precoders or the combiners is computed as the dominant eigenvector corresponding to the eigenvalue decomposition (EVD) of the channel correlation matrix (i.e., the sample covariance matrix). In addition to this, the easier implementation of the subarray structure simplifies the precoder and the combiner design to a block diagonal form, which incurs a lower computational complexity. Thus, for the subarray-based structure, RF variables are obtained using the correlation matrix of the sub-channel matrix corresponding to the antenna elements of the subarray. Note that EVD incurs a cubic computational overhead (say  $O(N^3)$ ). Thus, the subarray structure reduces the overhead to  $O((N/U)^3)$ . However, the optimal solution above needs to access the channel state information (CSI) of the large MIMO channel, which is unable to estimate in reality. Therefore, in this article, we assume the accurate knowledge of RF effective channel only, where the RF precoders and combiners are provided by genie. In practice, these RF quantities are obtained by beam-training codebooks [10]. Next, the optimal BB precoders/combiners can then be obtained as the left/right dominant singular vectors of the estimated RF effective channel matrix. Note that this BB transceiver design is applicable for the nodes, which have perfect interference cancellation or do not experience interference. However, in the IAB networks, there is strong SI presents at the IAB-node, needing cancellation. In thi case, the above hybrid design for the IAB-node needs to be modified.



(a)



(b)

Fig. 3. a) Multiuser hybrid transceiver for FD-IAB wideband mmWave system; b) subarray structure for multiuser transmission (8×8 UPA, 4 users).

### Multiuser Interference and Self-Interference Cancellation

To maximize the SE at the IAB-node receiver, the BB precoders/combiners at the IAB-node must achieve the following. The transceiver design should

- mitigate the RSI at the receiver of the IAB-node, and
- cancel the MUI at the transmitter of the IAB-node.

Technically, in mmWave, such a high-power SI is likely to exceed the limitation of the dynamic range on analog-to-digital converters (ADCs) and results in a strong non-linear signal than that of desire signal. Therefore, the antenna and the RF cancellation are adopted before the digital process to cancel out a large amount of SI [13]. However, the study in [3] states that for the mmWave wideband, the RF cancellation faces difficulties in the canceler design due to the realization of large number of taps and the high delay spread of the SI channel, and also experiences severe performance degradation due to RF impairments, as compared to that in the microwave communications. A wideband active analog SIC is studied in [14]. With this novel RF cancellation technique, those difficulties on traditional RF canceler design can be overcome.

Consequently, the remaining RSI will be handled by the digital cancellation, i.e., by applying the MMSE BB combiner at the IAB-node. In order to achieve a good digital SIC, the number of RF chains at the receiver of the IAB-node should be at least the sum of the number of data streams transmitted and received by the IAB-node. Since the BB SIC depends

on the estimated CSI of the SI channel, the CEE has a strong impact on the performance of digital SIC. A staged SIC which combines the RF and the digital cancellation is studied in our recent work [10]. Regarding the MUI, traditional ZF is utilized at the IAB-node transmitter based on the RF effective channel to obtain the desired BB precoder.

### RF Insertion Loss

The RFIL,  $L_{RF}$ , which is caused by PSs, power dividers (PDs), and power combiners (PCs), is an important loss that cannot be easily compensated by the existing technologies in the mmWave. Failure to take account of the RFIL may result in higher analytical spectral efficiency. To act the impact of the RFIL, the factor,  $1/\sqrt{L_{RF}}$ , is multiplied with the RF precoder/combiner matrices.

For the fully connected structure, the RF precoding requires  $N_{RF}$  PDs ( $N_t$ -way),  $N_t$  PCs ( $N_{RF}$ -way) and  $N_t N_{RF}$  PSs, while the RF combining needs  $N_r$  PDs ( $N_{RF}$ -way),  $N_{RF}$  PCs ( $N_r$ -way), and  $N_r N_{RF}$  PSs, where  $N_t$ ,  $N_r$  and  $N_{RF}$  denotes the number of transmitters, receivers, and RF chains, respectively.

On the other hand, for the RF precoding with  $U$  subarrays,  $U$  PDs ( $N_t/U$ -way) and  $N_t$  PSs are required, while at each subarray (user) of the receiver,  $U$  PCs ( $N_r/U$ -way) and  $N_r$  PSs are needed. Specially, at the receiver of the IAB-node,  $N_r$  PDs ( $N_{RF}/U$ -way),  $N_{RF} N_r/U$  PSs, and  $N_{RF}$  PCs ( $N_r/U$ -way) are required.

Given that a cascade of  $\lceil \log_2(X) \rceil$  stages of 2-way PDs and  $\lceil \log_2(Y) \rceil$  stages of 2-way PCs are utilized to construct the  $X$ -way PD and the  $Y$ -way PC, respectively.  $L_{RF}$  is given by the product of the static power loss of PDs (i.e.,  $P_D \lceil \log_2(X) \rceil$  dB), PSs (i.e.,  $P_{PS}$  dB), and PCs (i.e.,  $P_C \lceil \log_2(Y) \rceil$  dB), where  $P_D = 0.6$  dB and  $P_C = 3.6$  dB denote the power loss of the PD and the PC, respectively. Moreover, there are two kinds of PSs, i.e., the active PS ( $P_{PS} = -2.3$  dB) and the passive PS ( $P_{PS} = 8.8$  dB) [15].

### SIMULATION RESULTS

In this section, simulations are presented to analyze the SE for our hybrid precoding design with the impact of the CEE and the RFIL. The OFDM system has  $K = 512$  subcarriers, where each channel realization has  $D = 128$  delay taps. For a 4-subarray (user) hybrid precoding system, each subarray (user) has  $4 \times 16$  UPA with 1 RF chain and 1 data stream.

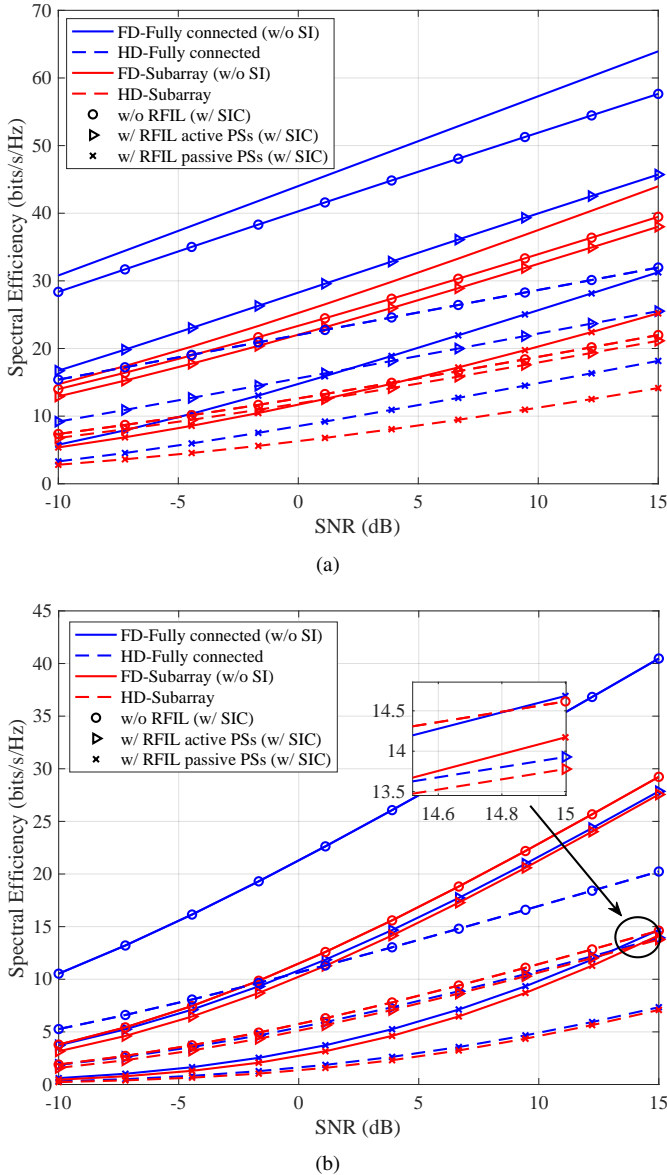


Fig. 4. Comparison of the impact of RFIL on the SE of a 4-user mmWave-IAB-FD system with different hybrid precoding structures in terms of different kinds of PSs. The number of subarrays is equal to that of the user: a) backhaul link:  $16 \times 16$  UPA, 4 (8) RF chains at Tx (Rx), 4 data streams; b) access link:  $16 \times 16$  UPA and 4 RF chains at the Tx. Each user is equipped with 1 RF chain and  $4 \times 16$  UPA and receives 1 data stream from Tx.

For successful digital cancellation, each subarray has 2 RF chains at the receiver of the IAB-node. We assume that an 80 dB SIC has been applied before the digital cancellation by the antenna and the analog cancellation [10]. We define  $\text{SNR} \triangleq P_r / \sigma_n^2$ , where  $P_r = P_t / \bar{P}L$  is the ratio between transmit power and average path loss according to the Friis' law, and  $\sigma_n^2$  denotes the Gaussian noise power.

#### A. Effect of RF Insertion Loss

Fig. 4 shows the SE of both the backhaul and the access link with different hybrid precoding schemes by comparing FD and HD transmission in the presence of the RFIL in terms of different kinds of PSs. Both subfigures show a similar trend. Without considering the impact of the RFIL, the SE with FD

transmission of the fully connected structure is much higher than that of the subarray structure, which has the difference of around 20 bits/s/Hz and 12 bits/s/Hz for the backhaul and the access links, respectively, at  $\text{SNR} = 15$  dB. For the HD scheme, this difference reduces to a half. However, in the presence of the RFIL, the SE obtained from the subarray structure is close to that given by the fully connected one, which means that our precoding scheme experiences less effect from the RFIL. Moreover, it can be seen that the use of active PSs can provide a higher SE than that with passive PSs; however, with more power consumption [15]. Specifically, for the backhaul link with ideal RF components, the SE of FD with SIC is close to the ideal one (i.e., with perfect SIC), which indicates the successful SIC.

#### B. Effect of Channel Estimation Error

We assume that only the RF effective SI channel is known with uncertainty. Therefore, only the backhaul link performance will be affected by the CEE. From Fig. 5, it can be observed that irrespective of the selection of PSs, the higher SNR shifts the SE intersection of FD and HD to the left. At the right of the intersection, the FD scheme has less SE as the HD due to the higher CEE. Moreover, compared with the fully connected structure, our subarray-based hybrid precoding scheme is more sensitive to the CEE. Therefore, more advanced techniques are needed to estimate the RF effective SI channel as accurately as possible. Further, interestingly, with passive PSs, the intersection points shifts to the right, as compared with that for active PSs, implying the more tolerance of the system with passive PSs. It can be noted that although the fully connected structure shows a better SE, yet the incurred hardware cost is much less for the subarray structure.

#### C. Effect of RF Chains on Digital SIC

In Fig. 6, the digital SIC ability in terms of the SE of the backhaul link is plotted with different numbers of RF chains at the IAB-node receiver. The fully connected hybrid precoding schemes are assumed to have 4 (8) RF chains at the transmitter (receiver). The ideal curves are plotted by assuming perfect SIC. It is evident that the ideal fully connected-based precoding provides a close performance to the ideal full digital scheme, and leaves a gap with respect to the ideal subarray-based precoding scheme. Regarding the digital cancellation ability of the subarray structure, the more RF chains at the receiver of the IAB-node, the more improvements in the SE can be seen and the smaller the SE difference with respect to the ideal subarray curves. At 15 dB SNR, with different numbers of RF chains at the receiver of the IAB-node ( $L = 2, 4, 8$  per subarray), the SE of deploying digital SIC is improved nearly 23%, 33%, and 34%, respectively, and the corresponding rate loss gets to around 4.7, 2.1, and 1 bit(s)/s/Hz, respectively.

#### CONCLUSION

In this article, we have presented the multiuser mmWave-IAB architecture according to the latest 3GPP standard

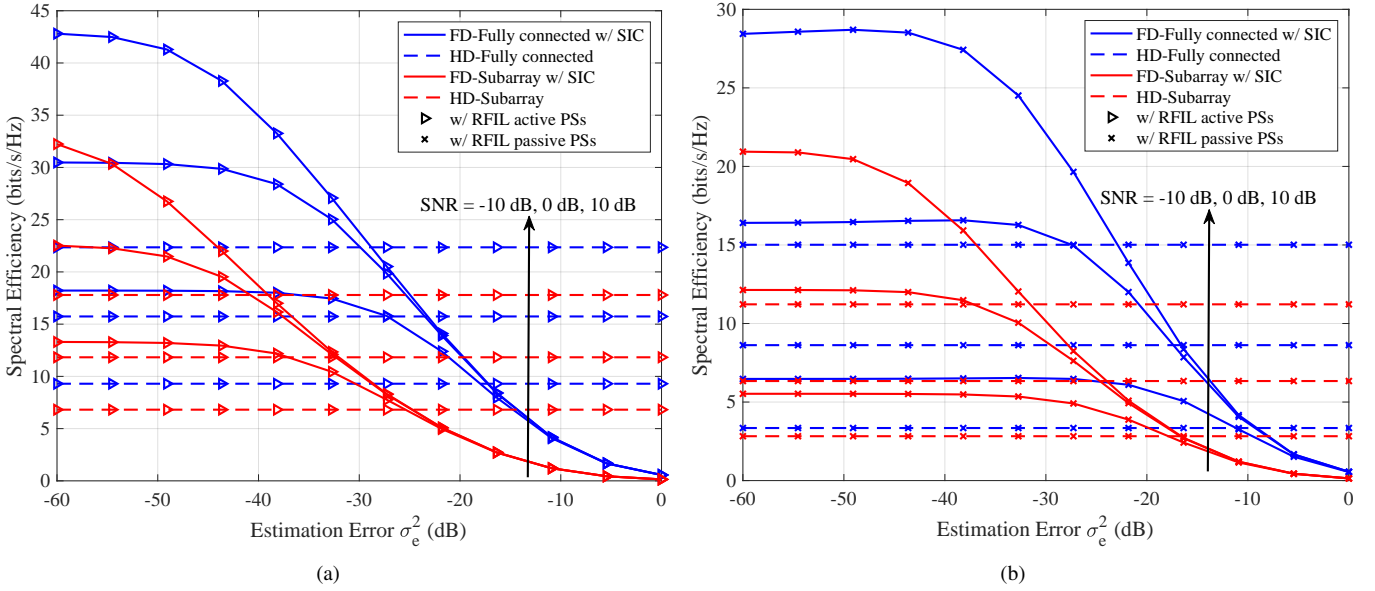


Fig. 5. Comparison of the impact of CEE on the backhaul link SE in the presence of RFIL of a 4-user mmWave-IAB-FD system with different hybrid precoding structures in terms of different SNR values. Equipped with  $16 \times 16$  UPA, 4 (8) RF chains at Tx (Rx), 4 data streams are transmitted. The number of subarrays is equal to that of the user: a) with active PSs; b) with passive PSs.

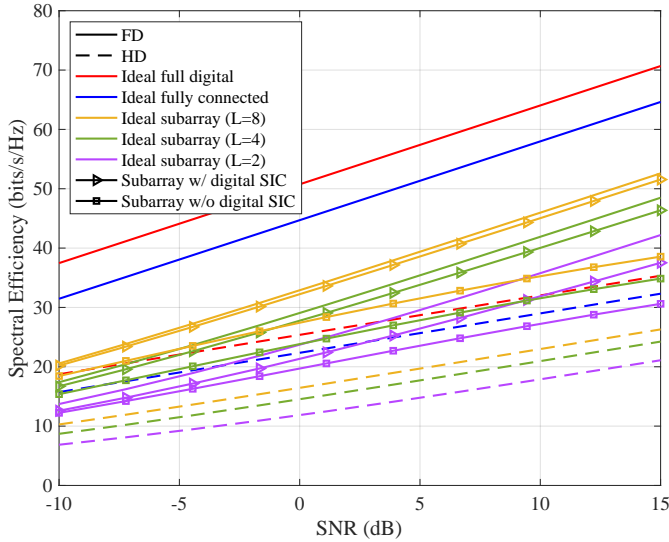


Fig. 6. Digital SIC ability of a 4-user wideband mmWave-FD-IAB subarray network in terms of different numbers of RF chains ( $L = 2, 4, 8$ ) on each Rx subarray. Equipped with  $16 \times 16$  UPA on both sides, 4 RF chains at Tx and 4 data streams are transmitted.

for the IAB networks. Wideband and FD operations have been investigated towards the SE perspective. Further, the general mmWave channel model is described, followed by the characterization of the SI channel for mmWave FD operation, including the challenges in the SI channel estimation. Through a hardware cost-effective and computationally efficient subarray-based hybrid precoding scheme, with the objective of SE maximization in the IAB networks, MUI and RSI are mitigated at the IAB-node transmitter and receiver using the BB ZF and MMSE, respectively. The impact of the RFIL with active or passive PSs has been analyzed. To

observe the effect of the imperfect RF effective CSI, the SE is plotted for different values of CEE in the presence of the RFIL, and compared with the HD operation. Simulations have shown that if the CEE is inversely proportional to SNR, the improvement of FD and HD can be observed. Moreover, the system with passive PSs can tolerate higher CEE than the system with active PSs.

Since the subarray hybrid precoding scheme is sensitive to the CEE, adjustments need to be investigated for accurate RF effective SI channel estimation. Further, equal power allocation assumption can be relaxed, and optimal power can be allocated to the effective channel. In practice, the PSs are not continuously controlled. Therefore, we will focus on quantization schemes with an efficient codebook design in the future. Moreover, an efficient antenna and RF cancellation are important to investigate to leverage the advantages of FD transmission.

## REFERENCES

- [1] S. Park, A. Alkhateeb, and R. W. Heath, "Dynamic Subarrays for Hybrid Precoding in Wideband mmWave MIMO Systems," *IEEE Trans. Wireless Commun.*, vol. 16, no. 5, pp. 2907–2920, May 2017.
- [2] O. Teyeb *et al.*, "Integrated Access Backhauled Networks," in *Proc. IEEE 90th Vehicular Technology Conference*, Honolulu, HI, USA, Sep. 2019.
- [3] Z. Xiao, P. Xia, and X. Xia, "Full-Duplex Millimeter-Wave Communication," *IEEE Wireless Commun. Mag.*, vol. 24, no. 6, pp. 136–143, Dec. 2017.
- [4] B. Lee *et al.*, "Reflected Self-Interference Channel Measurement for mmWave Beamformed Full-Duplex System," in *Proc. IEEE Globecom Workshops*, San Diego, CA, USA, Dec. 2015.
- [5] 3GPP, "NR; Study on Integrated Access and Backhaul," *TR 38.874 (Rel. 16)*, Dec. 2018.
- [6] —, "NG-RAN; Architecture Description," *TS 38.401 (Rel. 16)*, Sep. 2020.
- [7] O. Taghizadeh *et al.*, "Environment-Aware Minimum-Cost Wireless Backhaul Network Planning with Full-Duplex Links," *IEEE Syst. J.*, vol. 13, no. 3, pp. 2582–2593, Sep. 2019.

- [8] M. Polese *et al.*, "Integrated Access and Backhaul in 5G mmWave Networks: Potential and Challenges," *IEEE Commun. Mag.*, vol. 58, no. 3, pp. 62–68, March 2020.
- [9] A. Alkhateeb and R. W. Heath, "Frequency Selective Hybrid Precoding for Limited Feedback Millimeter Wave Systems," *IEEE Trans. Commun.*, vol. 64, no. 5, pp. 1801–1818, May 2016.
- [10] J. Zhang *et al.*, "Design and Analysis of Wideband Full-Duplex FR2-IAB Networks," *IEEE Trans. Commun.*, under review. [Online]. Available: [https://uoe-my.sharepoint.com/:f/g/personal/s1804540\\_ed\\_ac\\_uk/EuiTu5H9wnZP\pjEMB5eARuYBDOhJg2DlZNgxS3L5wCMhMg?e=v1B4c1](https://uoe-my.sharepoint.com/:f/g/personal/s1804540_ed_ac_uk/EuiTu5H9wnZP\pjEMB5eARuYBDOhJg2DlZNgxS3L5wCMhMg?e=v1B4c1)
- [11] K. Abbas *et al.*, "Joint Channel and Phase Noise Estimation for mmWave Full-Duplex Communication Systems," *EURASIP J. Adv. Signal Process.*, vol. 18, pp. 1–12, March 2019.
- [12] C. Masouros, M. Sellathurai, and T. Ratnarajah, "Vector Perturbation Based on Symbol Scaling for Limited Feedback MISO Downlinks," *IEEE Trans. Signal Process.*, vol. 62, no. 3, pp. 562–571, Feb. 2014.
- [13] L. Song, Y. Li, and Z. Han, "Resource Allocation in Full-Duplex Communications for Future Wireless Networks," *IEEE Wireless Commun. Mag.*, vol. 22, no. 4, pp. 88–96, Aug. 2015.
- [14] H. Luo, M. Holm, and T. Ratnarajah, "Wide-Band Active Analog Self-Interference Cancellation for 5G and Beyond Full-Duplex Systems," in *Proc. 54th Asilomar Conference on Signals, Systems and Computers*, Pacific Grove, CA, USA, Nov. 2020.
- [15] L. N. Ribeiro *et al.*, "Energy Efficiency of mmWave Massive MIMO Precoding with Low-Resolution DACs," *IEEE J. Sel. Topics Signal Process.*, vol. 12, no. 2, pp. 298–312, May 2018.

#### ACKNOWLEDGMENT

The work was supported in part by the research grant from Huawei Technologies (Sweden) AB.

#### BIOGRAPHIES

JUNKAI ZHANG [S'21] received his B.Eng. degree in Communication Engineering from Shenyang Ligong University, Shenyang, China, in 2018, and M.Sc. degree in Signal Processing and Communications, with Distinction, from The University of Edinburgh, Edinburgh, UK., in 2019. He is currently with the Institute for Digital Communications, The University of Edinburgh, Edinburgh, UK., as a Ph.D. candidate. His research interests include 5G and beyond wireless networks, millimeter-wave communications, full-duplex radio, and Massive MIMO.

NAVNEET GARG [S'15, M'19] received the B.Tech. degree in electronics and communication engineering from College of Science & Engineering, Jhansi, India, in 2010, and the M.Tech. degree in digital communications from ABV-Indian Institute of Information Technology and Management, Gwalior, in 2012. He completed the Ph.D. degree in June 2018 from the department of electrical engineering at the Indian Institute of Technology Kanpur, India. From July 2018-Jan 2019, he visited The University of Edinburgh, UK. From February 2019-2020, he was employed as a research associate in Heriot-Watt university, Edinburgh, UK. Presently, he is working as a research associate in The University of Edinburgh, UK. His main research interests include interference alignment, edge caching, optimization, and machine learning.

MARK HOLM [S'98, M'01] received his B.Sc. (hons) in Laser Physics and Optoelectronics from the University of Strathclyde in 1997, before studying for his Ph.D. in Physics from the University of Strathclyde which he received in

2001. He currently works as a technical lead and hardware system architect for Huawei Technologies (Sweden) AB with interests in microwave radio, phased array antennas, full duplex radio systems, and photonic radios. In the past, he was the microwave lead on AESA Radar systems, Senior Engineer responsible for GaAs pHEMT modeling, and also laser and package design engineer for SFP/XENPACK Fibre modules. He is published in the fields of laser design, and GaAs device modeling.

THARMALINGAM RATNARAJAH [S'94, A'96, M'05, SM'05] is currently with the Institute for Digital Communications, The University of Edinburgh, Edinburgh, U.K., as a Professor in digital communications and signal processing. He has supervised 15 Ph.D. students and 21 postdoctoral research fellows and raised more than 11+ million USD of research funding. He was the Coordinator of the EU projects ADEL (3.7M€) in the area of licensed shared access for 5G wireless networks, HARP (4.6M€) in the area of highly distributed MIMO, the EU Future and Emerging Technologies projects HIATUS (3.6M€) in the area of interference alignment, and CROWN (3.4M€) in the area of cognitive radio networks. His research interests include signal processing and information theoretic aspects of 5G and beyond wireless networks, full-duplex radio, mmWave communications, random matrix theory, statistical and array signal processing, and quantum information theory. He has published over 400 articles in these areas and holds four U.S. patents. He is a Fellow of the Higher Education Academy (FHEA). He was an Associate Editor of the IEEE TRANSACTIONS ON SIGNAL PROCESSING, from 2015 to 2017, and the Technical Co-Chair in the 17th IEEE International Workshop on Signal Processing Advances in Wireless Communications, Edinburgh, in 2016.